DALTON
FULL PAPER

Oxoanion influences on the self-assembly of cationic co-ordination complex polymers of the nickel(II)–di-4-pyridylamine family

Matthew C. Laskoski,[a] Robert L. LaDuca Jr.,*[a] Randy S. Rarig Jr.[b] and Jon Zubieta *[b]

[a] *Department of Chemistry and Physics, King's College, Wilkes-Barre, PA 18711, USA*
[b] *Department of Chemistry, Syracuse University, Syracuse, NY 13244, USA*

Received 14th May 1999, Accepted 13th July 1999

Hydrothermal reactions of Ni^{II}, di-4-pyridylamine (dpa) and the appropriate oxide yield materials of the Ni^{II}–organodiamine–EO_4^{2-} family. Specifically, reaction of $NiCl_2 \cdot 6H_2O$, dpa, and MoO_3 in water at 120 °C yielded $[Ni(dpa)_2(MoO_4)]$ **1**, while the reaction of $NiSO_4 \cdot 6H_2O$ and dpa in water at 120 °C gave $[Ni(dpa)(SO_4)(H_2O)] \cdot 2H_2O$ **2**. The structures reveal the dramatic influence of the anion identity and ligation modes in the $\{Ni(dpa)_n\}_n^{2n+}$ substructure. The structure of **1** is constructed from two motifs, two-dimensional $\{Ni(dpa)\}_n^{2n+}$ sheets and one-dimensional $\{NiMoO_4\}_n$ chains, to produce a three-dimensional covalently linked framework. In contrast, the $\{Ni(dpa)\}_n^{2n+}$ substructure of **2** is three-dimensional, with co-ordinated SO_4^{2-} and aqua ligands projecting into channels formed by the $\{Ni(dpa)\}_n^{2n+}$ framework. The void is reduced through the common characteristic of interpenetration, such that the structure of **2** exhibits two independent three-dimensional frameworks.

The influence of organic components in determining the microstructure of inorganic oxides has been established for materials as diverse as zeolites, mesoporous MCM-41 compounds, transition metal phosphates and the products of biomineralization.[1–8] While the organic component of such hybrid materials is most commonly incorporated as a charge compensating cation or as a ligand to the metal sites of the oxide framework itself, it may also participate in ligation to the metal center of a co-ordination complex cation, as in $[Cu(en)_2][V_6O_{14}]$.[9] A more recent and related approach relies on the exploitation of the organic component as a bridging ligand in the construction of polymeric co-ordination complex cations which serve not only as charge-compensating units but as a rigid scaffolding for the entraining of the anionic component. This approach is especially attractive since the intense activity in the field of crystal engineering has afforded numerous examples of cationic co-ordination complex polymers with one-, two-, and three-dimensional structures and a variety of architectural motifs for use in the self-assembly of the composite oxide materials.[10–13] Examples of this approach include $[\{Cu(4,4'\text{-bpy})\}_4Mo_{15}O_{47}]$,[14] $[Cu(dpe)(MoO_4)]$ (dpe = *trans*-1,2-bis(4-pyridyl)ethane),[15] and $[\{Cu_2(C_2H_2N_3)_2(H_2O)_2\}Mo_4O_{13}]$ ($C_2H_2N_3$ = triazolate).[16]

The structural systematics of these materials reveal a number of geometric determinants including the co-ordination preferences of the metals, the relative dispositions of the ligand donor groups, and the distance between donor groups. It is also apparent that the oxide component does not act simply as a passive constituent to be molded by the spatial requirements of the scaffolding provided by the polymeric cation, but rather exerts a synergistic influence at the structure-determining organic–inorganic interface. The anion influence on the polymer cation substructure is evident in the structures of $[Cu_2Br_2(C_2H_2N_3)]$,[17] $[Cu_3(C_2H_2N_3)_2V_4O_{12}]$,[18] and $[\{Cu_2(C_2H_2N_3)_2(H_2O)_2\}Mo_4O_{13}]$,[16] where one-, two-, and three-dimensional Cu–triazolate structures, respectively, are encountered. Since anion binding and the structure-determining role of anions has attracted some attention,[19] we have continued to explore the role of the anionic component in the self-assembly of materials constructed from polymeric co-ordination cations and simple oxoanions. The Ni^{II}–di-4-pyridylamine(dpa)–EO_4^{2-} system (E = S or Mo) has provided two unusual three-dimensional solids, $[Ni(dpa)_2(MoO_4)]$ **1** and $[Ni(dpa)_2(SO_4)(H_2O)] \cdot 2H_2O$ **2**, which illustrate the profound influence of the significantly greater basicity of molybdate relative to sulfate on the overall architecture of the solid. Anion binding and its structural influences as templates for the formation of supramolecular entities have attracted considerable comtemporary interest.[19,20] While most investigations have focused on hydrogen-bonding interactions between an organic host and an anionic guest, Lewis acid–base interactions between a metal cation and an anion have also been explored in the recent literature.[21–23]

Experimental

Syntheses were carried out in Parr acid digestion bombs with 23 ml poly(tetrafluoroethylene) liners or in borosilicate tubes with 5/8 in outside diameter, 3/32 in wall thickness, and 6 in length. The compounds $CuSO_4 \cdot 5H_2O$ and $NiCl_2 \cdot 6H_2O$ were purchased from Aldrich and used without further purification. Di-4-pyridylamine (dpa) was prepared by a published procedure.[24,25] Water was distilled above 0.3 MΩ in-house using a Barnstead model 525 Biopure Distilled water center. Infrared spectra were obtained on a Perkin-Elmer 1600 Series FTIR spectrometer.

Synthesis of $[Ni(dpa)_2(MoO_4)]$ 1

A solution of $NiCl_2 \cdot 6H_2O$ (0.132 g), MoO_3 (0.080 g), dpa (0.087 g), Et_4NOH (0.082 g) and water (10.00 g) in the mole ratio 1 : 1 : 1 : 1 : 1000 was heated at 120 °C for 72 h in a 23 ml Parr acid digestion bomb. After cooling to room temperature, blue crystals of compound **1** were isolated in 70% yield. Calc. for $C_{20}H_{18}MoN_6NiO_4$: C, 42.8; H, 3.21; N, 15.0. Found: C, 42.9; H, 3.04; N, 14.7%. IR (KBr pellet; cm^{-1}): 1590s, 1505m, 1345m, 1201m, 855s and 846 (sh). UV-visible (cm^{-1}): 16 100.

Synthesis of $[Ni(dpa)_2(SO_4)(H_2O)] \cdot 2H_2O$ 2

A solution of $NiSO_4 \cdot 6H_2O$ (0.088 g), dpa (0.057 g) and water (6.00 g) in the mole ratio 1 : 1 : 1000 was heated at 120 °C for 21 h in a borosilicate tube. After cooling to room temperature, light blue crystals of compound **2** were isolated in 60% yield. Calc. for $C_{20}H_{24}N_6NiO_7S$: C, 43.5; H, 4.35; N, 15.2. Found: C, 43.4; H, 4.25; N, 14.9%. IR (KBr pellet, cm^{-1}): 1583s, 1521s, 1340s (br), 1203m, 1082m, 1060m and 1009m. UV-visible (cm^{-1}): 16 000.

X-Ray crystallographic studies

Experimental single crystal X-ray diffraction data for structures **1** and **2** are displayed in Table 1, and selected bond lengths and angles are listed in Tables 2 and 3. Data collection was performed on a Siemens SMART diffractometer at 150 K with graphite monochromated Mo-Kα radiation ($\lambda = 0.71073$ Å), equipped with a CCD detector. Data were corrected for absorption using the ψ scan method and for Lorentz-polarization effects. Data processing was accomplished with the SAINT processing program.[26] Direct methods were used to solve all structures using the SHELXTL crystallographic software package.[27] All atoms except hydrogens were refined anisotopically. Neutral atom scattering factors were taken from Cromer and Waber,[28] and anomalous dispersion corrections were those of Creagh and McAuley.[29]

CCDC reference number 186/1597.

Results and discussion

While well established for the synthesis of zeolites, the hydrothermal method has more recently been adapted to the preparation of a wide variety of metastable materials, including transition metal phosphates[5,6] and even complex polyoxoalkoxometalates.[30] Hydrothermal reactions, typically carried out in the temperature range 120–260 °C under autogenous pressure, exploit the self-assembly of the product from soluble precursors.[31] The reduced viscosity of water under these conditions enhances diffusion processes so that solvent extraction of solids and crystal growth from solution are favored.[32] Since differential solubility problems are minimized, a variety of simple precursors may be introduced, as well as a number of organic and/or inorganic structure-directing agents from which those of appropriate size and shape may be selected for efficient crystal packing during the crystallization process. Under such non-equilibrium crystallization conditions, metastable kinetic phases rather than the thermodynamic phase are most likely isolated.[33] While several pathways, including that resulting in the most stable phase, are available in such non-equilibrium mixtures, the kinetically favored structural evolution results from the smallest perturbations of atomic positions. Consequently, nucleation of a metastable phase may be favored.

The reaction conditions employed for the preparations of compounds **1** and **2** were relatively simple. For the isolation of **1**, an aqueous mixture of dpa, $NiCl_2 \cdot 6H_2O$ and MoO_3 was adjusted to pH 5.5 by the addition of Et_4NOH and heated at 120 °C. Monophasic material was obtained in good yield. In the case of **2**, the optimum reaction conditions required the heating of a solution of dpa and $NiSO_4 \cdot 6H_2O$ in water without recourse to pH adjustment. Once again, the product formed in good yield as monophasic, crystalline material.

The infrared spectra of compounds **1** and **2** exhibit characteristic ligand bands at *ca.* 1590, 1500, 1340 and 1200 cm^{-1}. Compound **1** also possesses a strong intensity band at 855 cm^{-1} attributed to ν(Mo=O). In contrast, **2** displays a series of three bands at 1082, 1060, and 1009 cm^{-1}, a characteristic pattern for unidentate sulfate.[34] The diffuse reflectance spectra of **1** and **2** exhibit a strong UV band at *ca.* 37 000 cm^{-1} and a weak intensity transition centered at *ca.* 16 000 cm^{-1} which is presumably d–d in origin, arising from excitation from the $^3A_{28}$ ground state to a higher energy triplet state.

The structure of $[Ni(dpa)_2(MoO_4)]$ **1** consists of a covalently linked three-dimensional framework shown in Fig. 1. The fundamental building block is provided by the six-co-ordinate $\{Ni(dpa)_4(MoO_4)_2\}$ unit illustrated in Fig. 2(a). The nickel(II) center exhibits $\{NiN_4O_2\}$ co-ordination geometry by bonding to four nitrogen donors from each of four dpa ligands in the equatorial plane and two oxygen donors from two MoO_4^{2-} groups in the axial positions, so as to adopt D_{4h} local site symmetry. As shown in Fig. 3, the dpa ligands serve to bridge each

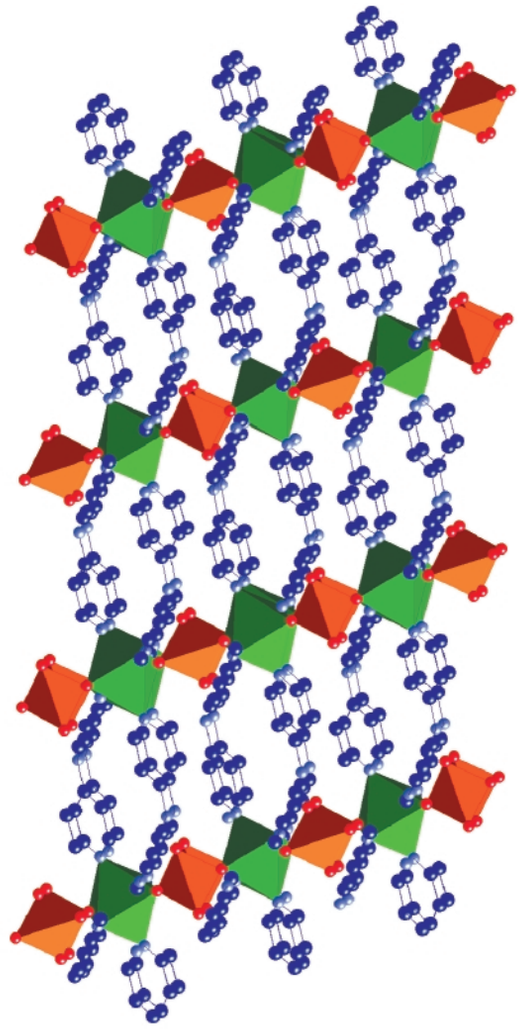

Fig. 1 A view of the three-dimensional structure of $[Ni(dpa)_2(MoO_4)]$ **1**. The nickel(II) octahedra and molybdenum(VI) tetrahedra are shown as green and orange polyhedra, respectively.

nickel(II) site to four adjacent nickel sites to form a two-dimensional $\{Ni(dpa)\}_n^{2n+}$ cationic network. The building block of this two-dimensional substructure is the $\{Ni_4(dpa)_4\}$ forty-membered ring.

The molybdate units adopt the μ-η^2-co-ordination mode to the Ni(II) sites and consequently form folded one-dimensional {Mo–O–Ni–O–Mo–} chains, shown in Fig. 3(b). Combining the two-dimensional $\{Ni(dpa)\}_n^{2n+}$ and the one-dimensional Ni–molybdate motifs results in the overall three-dimensional framework structure of Fig. 1. The structure is most conveniently described as $\{Ni(dpa)\}_n^{2n+}$ layers linked through $\{MoO_4\}^{2-}$ bridges into a three-dimensional framework. Alternatively, the structure may be viewed as $\{NiMoO_4\}$ chains linked through dpa bridges into a three-dimensional covalent framework. When viewed down the crystallographic *c* axis, that is along the $\{NiMoO_4\}$ chains, the "starburst" structural motif is quite evident (Fig. 4). The structure adopted by **1** results in efficient packing in the crystal. The consequences of this are the absence of interpenetration of independent substructures, a common phenomenon in open framework structures with large void volumes,[11] and the absence of solvent molecules of crystallization due to the restricted void volume associated with **1**. This observation is in stark contrast to the structure of **2**, which as described below adopts an open framework adamantoid cage, with concomitant two-fold interpenetration and encapsulation of water molecules into the significant void volume.

In contrasting the structure of compound **1** to the single other example of a material of the M^{II}–dpa–molybdate class reported to date, the copper(II) derivative $[Cu(dpa)_{0.5}(MoO_4)]$,[30]

Table 1 Summary of crystal data and experimental conditions for the X-ray study of $[Ni(dpa)_2(MoO_4)]$ **1** and $[Ni(dpa)_2(SO_4)(H_2O)]\cdot 2H_2O$ **2**

	1	**2**
Chemical formula	$C_{20}H_{18}MoN_6NiO_4$	$C_{20}H_{24}N_6NiO_7S$
M	561.06	551.22
Crystal system	Monoclinic	Orthorhombic
Space group	$C2/c$	$Pca2_1$
a/Å	19.2013(11)	15.0958(2)
b/Å	10.2785(6)	17.0071(1)
c/Å	11.984(7)	17.4842(2)
β/°	107.141(1)	
V/Å^3	2260.1(2)	4488.82(8)
D_c/g cm^{-3}	1.649	1.631
Z	4	8
Reflections collected, observed	2645, 2645	8632, 8632
μ/cm^{-1}	14.26	10.14
$R1$	0.0342	0.0266
$wR2$	0.0610	0.0686

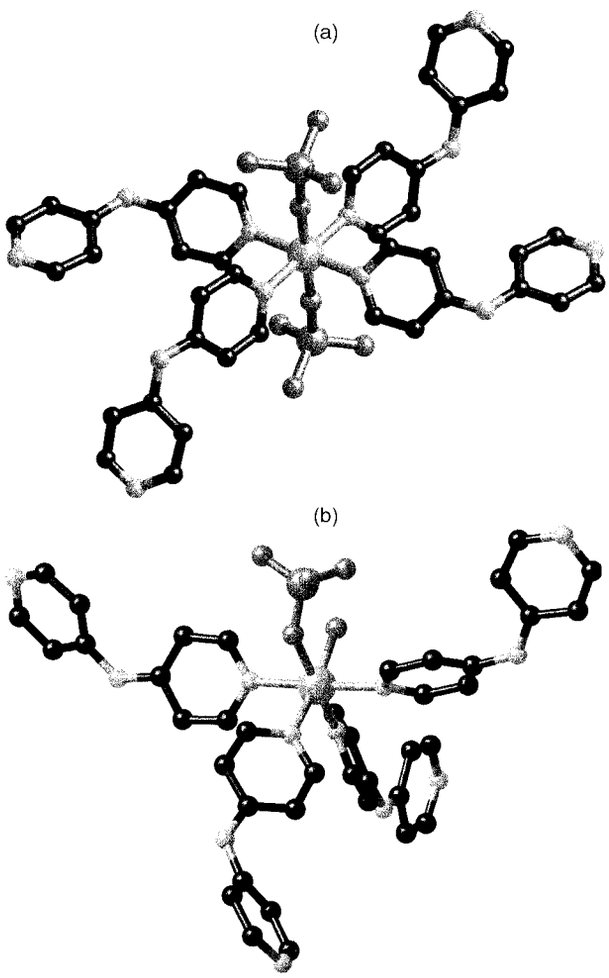

Fig. 2 (a) A view of the $\{Ni(dpa)_4(MoO_4)_2\}$ building block of compound **1**. (b) A view of the $\{Ni(dpa)_4(SO_4)(H_2O)\}$ building block of **2**.

the structural role of the co-ordination preferences of the metal are apparent. The copper(II) sites of $[Cu(dpa)_{0.5}(MoO_4)]$ adopt axially distorted $\{CuO_5N\}$ six-co-ordinate geometry, which results in a bimetallic oxide layer structure constructed from edge-sharing tetranuclear copper(II) subunits linked by $\{MoO_4\}^{2-}$ tetrahedra. The dpa groups project above and below a layer and link adjacent layers into the three-dimensional framework structure shown in Fig. 5. The distinctive structures adopted by $[Cu(dpa)_{0.5}(MoO_4)]$ and $[Ni(dpa)(MoO_4)]$ emphasize the role played by co-ordination preferences of the

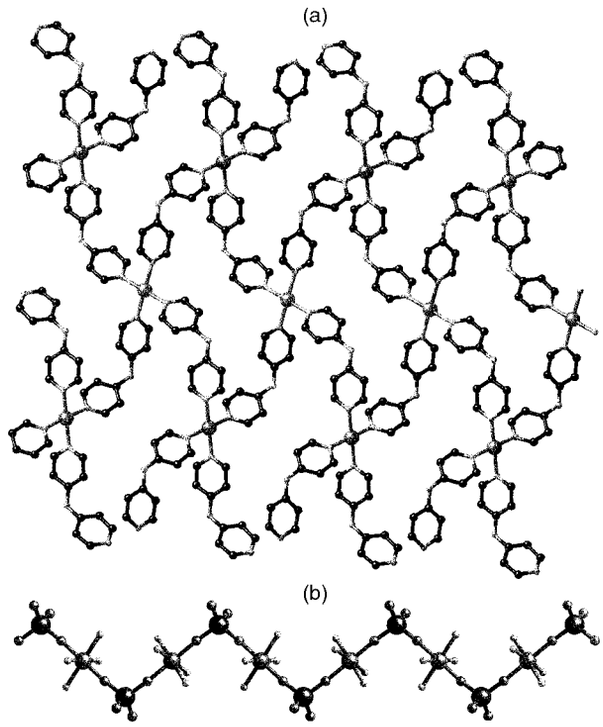

Fig. 3 (a) A view of the two-dimensional $\{Ni(dpa)_2\}_n^{2n+}$ network of compound **1**. (b) The folded one-dimensional $\{NiMoO_4\}$ chain of **1**.

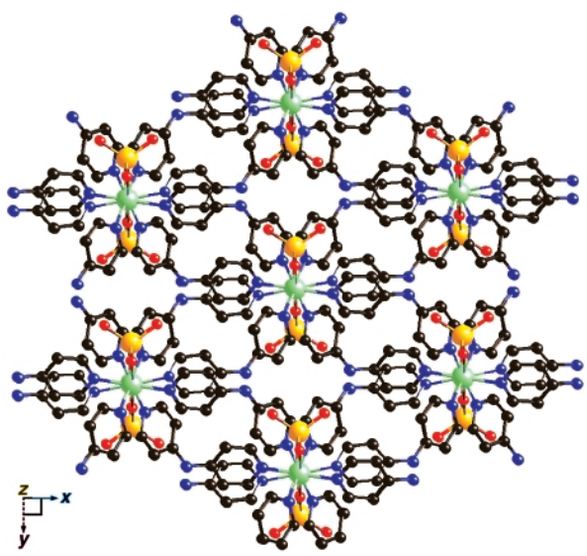

Fig. 4 A view of the structure of compound **1** parallel to the c axis and to the $\{NiMoO_4\}$ chains, showing the "starburst" motif.

metal(II) centers on the architecture of the $\{M(dpa)\}_n^{2n+}$ substructure of the solid. Attempts to prepare other materials of the type $[M^{II}(dpa)(MoO_4)]$, which are structurally analogous to the nickel(II) derivative **1**, have proved unsuccessful.

The structural consequences of replacing molybdate by sulfate in the Ni^{II}–dpa–EO_4^{2-} system are dramatic, as illustrated in Fig. 6 for the structure of $[Ni(dpa)_2(SO_4)(H_2O)]\cdot 2H_2O$ **2**. The fundamental unit in this instance is the distorted six-co-ordinate $\{Ni(dpa)_4(SO_4)(H_2O)\}$ illustrated in Fig. 2(b). This contrasts in several important respects with the $\{Ni(dpa)_4(MoO_4)_2\}$ unit of **1**. Rather than assuming the $\{Ni(dpa)_4(EO_4)_2\}$ core of **1**, compound **2** exhibits a $\{Ni(dpa)_4(EO_4)(H_2O)\}$ core, with replacement of one EO_4 group by an aqua ligand. Furthermore, the SO_4^{2-} and aqua ligands are disposed *cis* in **2**, resulting in C_{2v} local site symmetry for the $\{NiN_4O_2\}$ co-ordination polyhedron in place of the D_{4h} site symmetry of **1**.

Table 2 Selected bond lengths (Å) and angles (°) for $[Ni(dpa)_2(MoO_4)]$ **1**

Mo(1)–O(2)	1.757(2)	Mo(1)–O(2)	1.757(2)
Mo(1)–O(1)	1.7675(14)	Mo(1)–O(1)	1.7675(14)
Ni(2)–O(1)	2.0260(14) × 2	Ni(2)–N(1)	2.134(2) × 2
Ni(2)–N(3)	2.119(2) × 2		
O(2)–Mo(1)–O(2)	111.42(11)	O(1)–Mo(1)–O(1)	109.33(10)
O(2)–Mo(1)–O(1)	108.51(7) × 2	N(3)–Ni(2)–N(3)	180.0
O(2)–Mo(1)–O(1)	109.52(7) × 2	Mo(1)–O(1)–Ni(2)	175.37(9)
O(1)–Ni(2)–O(1)	180.0	N(3)–Ni(2)–N(1)	84.71(6) × 2
O(1)–Ni(2)–N(3)	90.93(6) × 2	O(1)–Ni(2)–N(1)	89.98(6) × 2
O(1)–Ni(2)–N(3)	89.07(6) × 2	N(3)–Ni(2)–N(1)	95.29(6) × 2
O(1)–Ni(2)–N(1)	90.02(6) × 2	N(1)–Ni(2)–N(1)	180.0

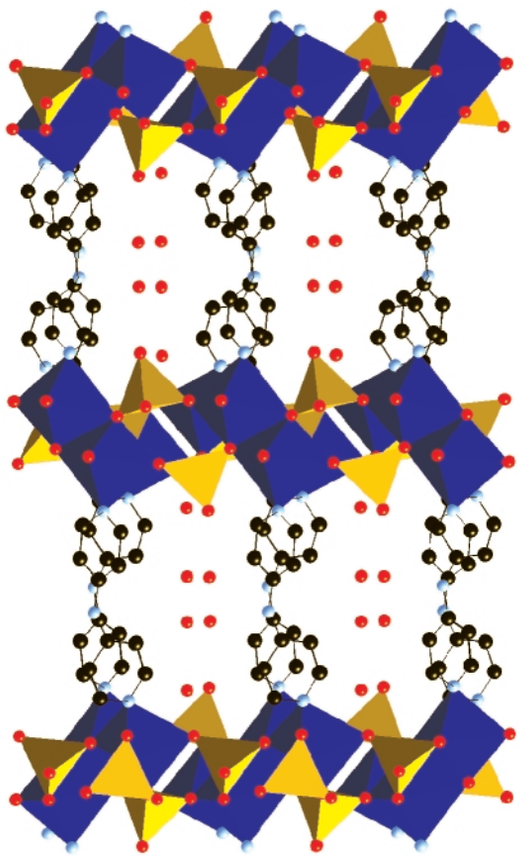

Fig. 5 A view of the structure of $[Cu(dpa)_{0.5}(MoO_4)]$, showing the $\{CuMoO_4\}$ bimetallic oxide layers linked by bridging dpa ligands into a three-dimensional framework. The copper(II) octahedra and molybdenum(VI) tetrahedra are displayed as blue and yellow polyhedra, respectively. The red spheres occupying the interlamellar regions are water molecules of crystallization.

The four dpa ligands about a given nickel(II) site of compound **2** bridge to four adjacent sites, two in a sheet parallel to the *ab* plane and one above and below the plane. Consequently, the $\{Ni(dpa)\}_n^{2n+}$ substructure of **2** is three-dimensional, in contrast to the two-dimensional substructure of **1**. The structure may be described as two-dimensional $\{Ni(dpa)_2\}_n^{2n+}$ sheets, parallel to the *ab* plane linked to adjacent sheets through dpa bridging ligands. The sheet motif is constructed from $\{Ni_6(dpa)_6\}$ fused rings. The sulfate group is monodentate and terminal, in contrast to the bidentate bridging mode assumed by $\{MoO_4\}^{2-}$ in **1**. Both the $\{SO_4\}^{2-}$ group and the aqua ligand project into the channels formed by the stacking of the sheets.

As shown in Fig. 7, the three-dimensional framework of compound **2** is constructed from adamantoid cages and is thus topologically related to the structures of such diimine bridged species as $[Ag(4,4'\text{-bpy})_2][CF_3SO_3]$,[35] $[Cu(4,4'\text{-bpy})_2]PF_6$,[36] $[Cu(3,3'\text{-bpy})_2]BF_4$,[37] $[CuL_2]BF_4$ [L = 1,2-bis(4-pyridyl)-ethane][38] and $[CuL']PF_6$ (L′ = 2,7-diazapyrene).[39] The diamondoid cage is considerably distorted from its idealized geometry as a consequence of the disposition of the dpa nitrogen donors about a distorted octahedral nickel(II) site rather than an idealized tetrahedral mode and also by virtue of the non-linearity of the dpa ligand in contrast to the rigid linear tethers in 4,4′-bpy.

It is also noteworthy that the structure of compound **2** consists of two independent and interpenetrating diamondoid frameworks, Fig. 8. The Ni···Ni interframe separation is 6.46 Å, while the intraframe Ni···Ni distance is 11.23 Å. These values may be compared to intraframe and interframe Ag···Ag distances of 9.93 and 4.82 Å, respectively, for $[Ag(4,4'\text{-bpy})_2]BF_4$. The latter contains four independent interwoven diamondoid frameworks, rather than the two exhibited by **2**.

Table 3 Selected bond lengths (Å) and angles (°) for $[Ni(dpa)_2(SO_4)(H_2O)]\cdot 2H_2O$ **2**

Ni(1)–N(4)	2.096(2)	Ni(1)–N(3)	2.114(2)
Ni(1)–O(5)	2.116(2)	Ni(1)–N(7)	2.145(2)
Ni(1)–N(1)	2.148(2)	Ni(1)–O(4)	2.180(2)
Ni(2)–N(10)	2.097(2)	Ni(2)–N(9)	2.107(2)
Ni(2)–O(9)	2.117(2)	Ni(2)–N(6)	2.125(2)
Ni(2)–O(10)	2.133(2)	Ni(2)–N(12)	2.134(2)
S(1)–O(2)	1.472(2)	S(1)–O(3)	1.481(2)
S(1)–O(1)	1.493(2)	S(1)–O(4)	1.503(2)
S(2)–O(6)	1.479(2)	S(2)–O(8)	1.480(2)
S(2)–O(9)	1.499(2)	S(2)–O(7)	1.503(2)
N(4)–Ni(1)–N(3)	89.92(8)	N(4)–Ni(1)–O(5)	172.05(9)
N(3)–Ni(1)–O(5)	86.92(7)	N(4)–Ni(1)–N(7)	92.99(8)
N(3)–Ni(1)–N(7)	177.02(8)	O(5)–Ni(1)–N(7)	90.11(7)
N(3)–Ni(1)–O(5)	98.21(8)	N(3)–Ni(1)–N(1)	89.07(8)
N(3)–Ni(1)–O(5)	89.04(7)	N(7)–Ni(1)–N(1)	91.14(8)
N(3)–Ni(1)–O(5)	86.18(7)	N(3)–Ni(1)–O(4)	89.30(8)
N(3)–Ni(1)–O(5)	86.49(7)	N(7)–Ni(1)–O(4)	90.26(8)
N(3)–Ni(1)–O(5)	175.32(7)	N(10)–Ni(2)–N(9)	89.66(8)
N(3)–Ni(1)–O(5)	86.30(8)	N(9)–Ni(2)–O(9)	86.45(8)
N(3)–Ni(1)–O(5)	177.77(8)	N(9)–Ni(2)–N(6)	92.24(8)
N(3)–Ni(1)–O(5)	92.65(8)	N(10)–Ni(2)–O(10)	87.56(7)
N(3)–Ni(1)–O(5)	171.30(8)	O(9)–Ni(2)–O(10)	85.15(7)
N(6)–Ni(2)–O(10)	90.40(7)	N(10)–Ni(2)–N(12)	88.17(8)
N(9)–Ni(2)–N(12)	99.38(8)	O(9)–Ni(2)–N(12)	171.95(7)
N(6)–Ni(2)–N(12)	92.67(8)	O(10)–Ni(2)–N(12)	88.77(7)
S(1)–O(4)–Ni(1)	135.95(11)	S(2)–O(9)–Ni(2)	137.15(11)

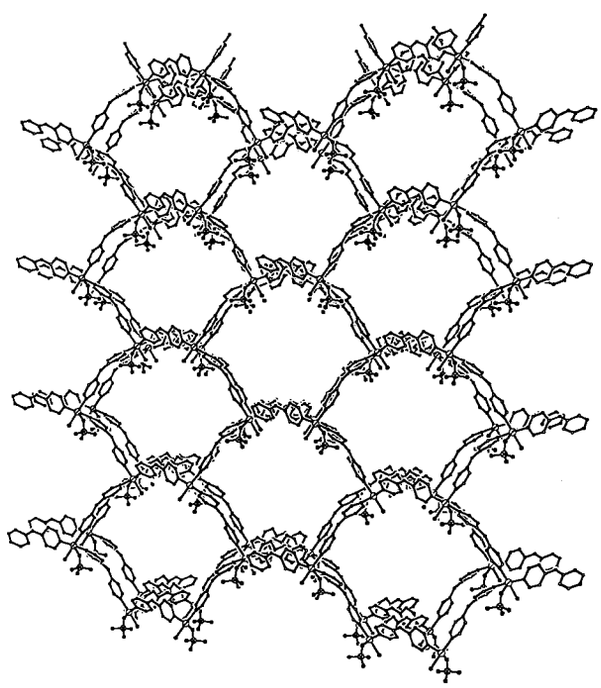

Fig. 6 A view of one of the two independent and interpenetrating three-dimensional frameworks of $[Ni(dpa)_2(SO_4)(H_2O)]\cdot 2H_2O$.

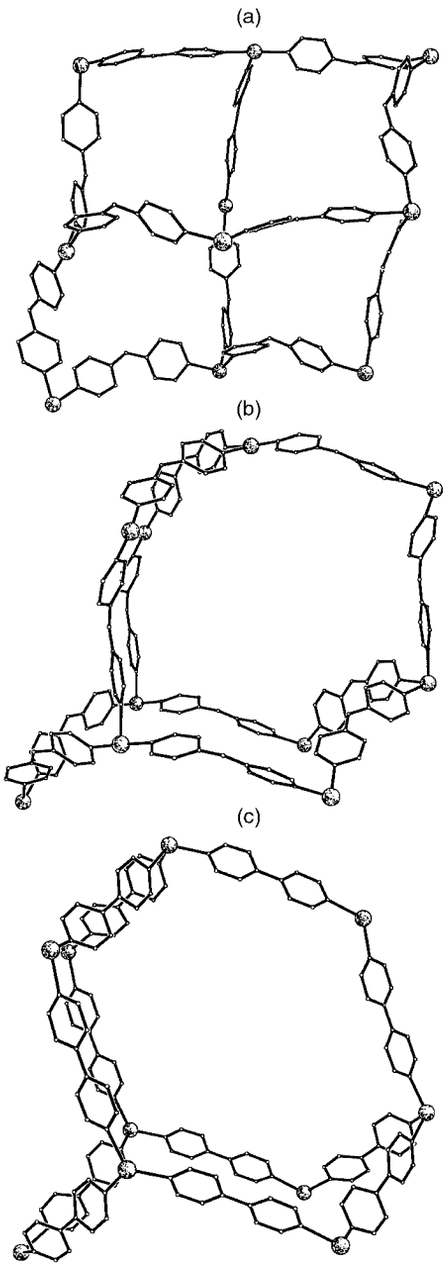

Fig. 7 Two views, (a) and (b), of the adamantoid cage of compound **2**; (c) the adamantoid cage of $[Ag(4,4'\text{-bpy})_2][CF_3SO_3]$.

The considerable void space associated with **2** is occupied by the sulfate and aqua ligands to the octahedral nickel(II) sites and by the two molecules of water of crystallization per Ni^{II} entrapped within the cages. The sulfate oxygen atoms and the aqua ligands form hydrogen-bonding interactions between the two independent frameworks. The water molecules of crystallization form an extensive hydrogen-bonded network among themselves and to the terminal oxo-groups of the sulfate ligands, Fig. 9.

Physical properties

The thermal decomposition of compound **1** exhibits a weight loss between 220 and 260 °C corresponding to the loss of the dpa ligand and yielding an amorphous blue material analysing for $CuMoO_4$. The thermogravimetric analysis of **2** reveals successive weight losses between 80–120 and 180–220 °C, corresponding to the loss of two water molecules of crystallization and a single co-ordinated water molecule, respectively. A further weight loss at 250–280 °C is attributed to the loss of the dpa ligand.

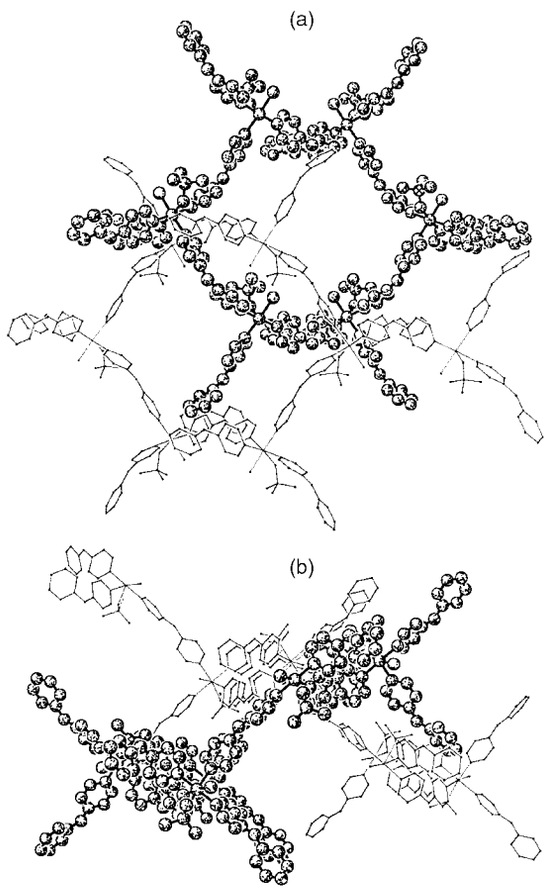

Fig. 8 Two views of the interpenetration of three-dimensional motifs in compound **2**.

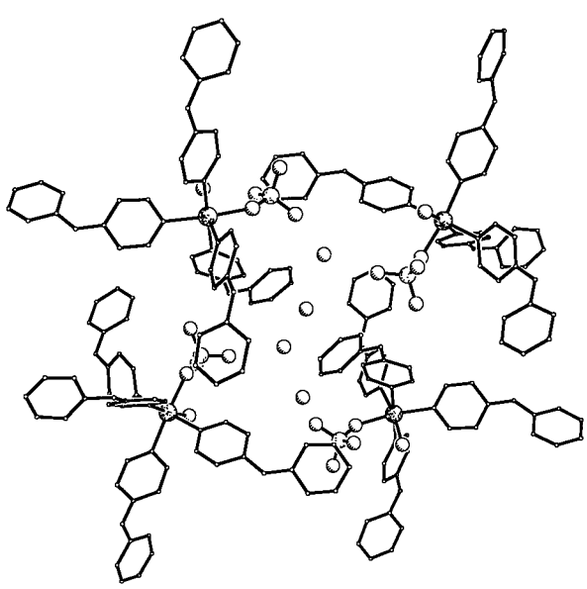

Fig. 9 A view of the cavity formed by four $\{Ni(dpa)_4(SO_4)(H_2O)\}$ segments, two from each of two adjacent independent frameworks.

Water sorption isotherms of dehydrated compound **2** exhibited Type I character,[40] consistent with accessibility of the internal pore volume of this material to the water substrate molecules, that is microporosity. In view of the acentricity of the structure of **2**, the dehydrated material was exposed to the NLO-active organic chromophore 2-nitroaniline. The expectation was that lattice inclusion would align the dipole moments of the organic substrate without recourse to electric field polling.[41] However, Kurtz powder measurements on the 2-nitroaniline inclusion compound were not feasible due to the strong

absorption of the inorganic framework which provided no window to observe the frequency doubling.[42]

Conclusions

The isolation of $[Ni(dpa)_2(MoO_4)]$ **1** and $[Ni(dpa)_2(SO_4)(H_2O)]\cdot 2H_2O$ **2** demonstrates the power of hydrothermal techniques for the preparation of organic–inorganic hybrid materials. The hydrothermal method provides a routine approach for the crystallization of phases constructed from polymeric co-ordination complex cations and a variety of anions. The strategy allows an elaboration of the structural systematics resulting from the synergistic interaction of the structurally diverse family of cationic framework materials with oxoanions of molecular one-, two-, and three-dimensional extensions.

The structures of compounds **1** and **2** reveal the interplay of various determinants. Thus, the architecture of the $\{Ni(dpa)\}_n^{2n+}$ scaffolding reflects, in part, the co-ordination preferences of the metal, the spacing between the nitrogen donors, and the ligand geometry. Furthermore, it is evident that the nature of the anion profoundly influences the overall architecture of the solid.

Compound **2** exhibits the diamondoid structure of the polymeric co-ordination cation, which represents a recurring theme of the structural chemistry of such frameworks. The flexibility of the co-ordination geometry about the six-co-ordinate nickel(II) site allows *cis* dispositions of the sulfate oxygen and aqua donors which results in an appropriate orientation of the dpa ligands for construction of the distorted adamantoid cages.

In contrast, the introduction of the molybdate anion in place of sulfate in compound **1** results in a two-dimensional $\{Ni(dpa)\}_n^{2n+}$ network. Once again, the co-ordination flexibility of the nickel(II) center allows a *trans* disposition of the molybdate groups. Furthermore, the tendency of molybdate units in structures of this type to bridge metal(II) centers provides a one-dimensional $\{NiMoO_4\}$ substructure which combines with the $\{Ni(dpa)\}_n^{2n+}$ network to form the three-dimensional structure of **1**.

Acknowledgements

This work was supported by National Science Foundation Grant CHE9617232 and by an award from the Research Corporation and a King's College Faculty Development Grant.

References

1 S. I. Stupp and P. V. Braun, *Science*, 1997, **277**, 1242.
2 J. V. Smith, *Chem. Rev.*, 1988, **88**, 149.
3 M. L. Occelli and H. C. Robson, *Zeolite Synthesis*, American Chemical Society, Washington, DC, 1989.
4 C. T. Kresge, M. E. Leonowicz, W. J. Roth, J. C. Vartuli and J. S. Beck, *Nature* (*London*), 1992, **359**, 710.
5 R. C. Haushalter and L. A. Mundi, *Chem. Mater.*, 1992, **4**, 31.
6 M. I. Khan, L. M. Meyer, R. C. Haushalter, C. L. Schweitzer, J. Zubieta and J. L. Dye, *Chem. Mater.*, 1996, **8**, 43.
7 S. Mann, S. L. Burkett, S. A. Davis, C. E. Fowler, N. H. Mendelson, S. D. Sims, D. Walsh and N. T. Whilton, *Chem. Mater.*, 1997, **9**, 2300.
8 L. L. Hench, *ACS Symp. Ser.*, 1995, **245**, 523.
9 Y. Zhang, J. R. D. DeBord, C. J. O'Connor, R. C. Haushalter, A. Clearfield and J. Zubieta, *Angew. Chem.*, *Int. Ed. Engl.*, 1996, **35**, 989.
10 D. Hagrman, P. Zapf and J. Zubieta, *Angew. Chem.*, *Int. Ed.*, 1999, **38**, in the press.
11 S. R. Batten and R. Robson, *Angew. Chem.*, *Int. Ed.*, 1998, **37**, 1460.
12 M. Bartelli, L. Carlucci, G. Ciani, D. M. Proserpio and A. Sironi, *J. Mater. Chem.*, 1997, **7**, 1271 and refs. therein.
13 P. Losier and M. J. Zaworotko, *Angew. Chem.*, *Int. Ed. Engl.*, 1996, **35**, 2779 and refs. therein.
14 D. Hagrman, C. Zubieta, D. J. Rose and R. C. Haushalter, *Angew. Chem.*, *Int. Ed. Engl.*, 1997, **36**, 795.
15 D. Hagrman, R. C. Haushalter and J. Zubieta, *Chem. Mater.*, 1998, **10**, 361.
16 D. Hagrman and J. Zubieta, *Chem. Commun.*, 1998, 2005.
17 R. Hammond and J. Zubieta, unpublished results.
18 P. J. Zapf and J. Zubieta, unpublished results.
19 R. Viler, D. M. P. Mingos, A. J. P. White and D. J. Williams, *Angew. Chem.*, *Int. Ed.*, 1998, **37**, 1258 and refs. therein.
20 G. Bianchi, E. Garcia-España and K. Bowman-James, *Supramolecular Chemistry of Anions*, Wiley-VCH, Wienheim, 1997.
21 S. Mann, G. Huttner and L. Zsolnai, *Angew. Chem.*, *Int. Ed. Engl.*, 1996, **35**, 2808.
22 X. Yang, C. B. Knoblen and M. F. Hawthorne, *Angew. Chem.*, *Int. Ed. Engl.*, 1991, **30**, 1507.
23 A. Muller, R. Sessoli, E. Krickemeyer, H. Bögge, J. Meyer, D. Gatteschi, L. Pardi, J. Westphal, K. Hovemeier, R. Rohlfing, J. Döring, F. Hellwig, C. Beugholt and M. Schmidtmann, *Inorg. Chem.*, 1997, **36**, 5329.
24 E. Koenigs and G. Jung, *J. Prakt. Chem.*, 1933, **137**, 141.
25 P. J. Zapf, R. L. LaDuca, Jr., R. S. Rarig, Jr., K. M. Johnson III and J. Zubieta, *Inorg. Chem.*, 1998, **37**, 3411.
26 SMART and SAINT, Siemens Analytical X-Ray Instruments Inc., Madison, WI, 1990.
27 SHELXTL, Version 5, Siemens Industrial Automation, Inc., Madison, WI, 1994.
28 D. T. Cromer and J. T. Waber, *International Tables for X-Ray Crystallography*, Kynoch Press, Birmingham, 1974, vol. IV, Table 2.2A.
29 D. C. Creagh and J. W. J. McAuley, *International Tables for X-Ray Crystallography*, Kluwer, Boston, MA, 1992, vol. C, Table 4.2.6.8.
30 M. I. Khan and J. Zubieta, *Prog. Inorg. Chem.*, 1995, **43**, 1.
31 A. Rabenau, *Angew. Chem.*, *Int. Ed. Engl.*, 1985, **24**, 1026.
32 R. A. Laudise, *Chem. Eng. News*, 1987, 28th September, 30.
33 J. Gopalakrishnan, *Chem. Mater.*, 1995, **7**, 1265.
34 K. Nakamoto, *Infrared Spectra of Inorganic and Co-ordination Compounds*, 2nd edn., Wiley-Interscience, New York, 1970, pp. 173–175.
35 L. Carlucci, G. Ciani, D. M. Proserpio and A. Sironi, *J. Chem. Soc.*, *Chem. Commun.*, 1994, 2755.
36 L. R. MacGillivray, S. Subramanian and M. J. Zaworotko, *J. Chem. Soc.*, *Chem. Commun.*, 1994, 1325.
37 S. Lopez, M. Kahraman, M. Harmata and S. W. Keller, *Inorg. Chem.*, 1997, **36**, 6138.
38 A. J. Blake, N. R. Champness, S. S. M. Chung, W.-S. Li and M. Schröder, *Chem. Commun.*, 1997, 1005.
39 A. J. Blake, N. R. Champness, A. N. Khlobystov, D. A. Lemenovskii, W.-S. Li and M. Schröder, *Chem. Commun.*, 1997, 1339.
40 D. M. Ruthven, *Principles of Adsorption and Absorption Processes*, Wiley, New York, 1984.
41 S. D. Huang and R.-G. Xiong, *Polyhedron*, 1997, **16**, 3929.
42 S. K. Kurtz and T. T. Perry, *J. Appl. Phys.*, 1968, **39**, 3798.

Paper 9/03880I